IEEE Access
Multidisciplinary | Rapid Review | Open Access Journal

Received 26 November 2022, accepted 10 December 2022, date of publication 12 December 2022,
date of current version 19 December 2022.

Digital Object Identifier 10.1109/ACCESS.2022.3228833

RESEARCH ARTICLE

Graphene-Metal Metasurface for Cloaking of Cylindrical Objects at Low-Terahertz Frequencies

SHEFALI PAWAR[1], (Student Member, IEEE), HOSSEIN MEHRPOUR BERNETY[2], (Member, IEEE), AND ALEXANDER B. YAKOVLEV[1], (Senior Member, IEEE)

[1]Department of Electrical and Computer Engineering, The University of Mississippi, University, MS 38677, USA
[2]Department of Mechanical Engineering, Stanford University, Stanford, CA 94305, USA

Corresponding author: Shefali Pawar (sbpawar@go.olemiss.edu)

This work was supported in part by the NSF Industry/University Cooperative Research Centers (I/UCRC) under Grant 1822104 and in part by Intel Corporation.

ABSTRACT Most of the theoretical studies involving graphene, typically assume an ultra-high mobility and/or high value of Fermi energy to achieve exciting functionalities such as polarization conversion, absorption, cloaking, among others. In practice, however, graphene with such high mobility is very difficult to realize, on account of the numerous flaws and impurities that inevitably are introduced during the graphene growth and transfer process. This severely compromises graphene's practical performance, despite the appeal of theoretical predictions. A novel design was presented in 'X. Wang et al., IEEE Trans. Antenna Propagat., vol. 67, pp. 2452–2461, 2019', wherein a graphene metasurface was devised to accomplish perfect absorption with excellent electrical tunability, for a wide span of practical mobility values for graphene (2,000 to 20,000 $cm^2V^{-1}s^{-1}$). Motivated by this design, in this paper, we introduce a graphene-metal metasurface structure, which is engineered to facilitate the realization of practical cloaking of conducting cylindrical objects. Though the framework for our cloak is ostensibly similar to the metasurface structure in the aforementioned reference, the phenomenon that our structure is based on, is radically different; consequently, the functionality and the numerical analysis differs. When this specific metasurface is enveloped around the cylindrical objects, their scattering width reduces noticeably, thereby making them 'invisible' to the impinging plane wave. Our design demonstrates cloaking even for the most practical low-mobility graphene, utilizing extremely low Fermi energy values, thereby making our construct desirable not only in theory, but also feasible for practical applications.

INDEX TERMS Complex surface conductivity, graphene-metal metasurface, low-mobility graphene, mantle cloaking.

I. INTRODUCTION

The allure of invisibility has galvanized the scientific community into focusing substantial amount of research and experimentations on achieving this phenomenon. In this regard, the concept of cloaking was established, which in general, is a surrounding cover responsible for curtailing scattered electromagnetic fields from an object in the near as well as the far-field regions. Several approaches have been reported over the past couple of decades, which deal with the design and analysis of different cloak structures. Transformation optics is one of the most prevalent methods [1], [2], [3], [4], [5], [6], [7]; alternative techniques include plasmonic cloaking [8], [9], [10], cylindrical transmission-line cloaking [11], [12], [13], among others. However, there are certain challenges involved with these methods, such as, the necessity of complex bulk volumetric metamaterials and the use of very high refractive index profiles for the cloak. As such, a different technique based on the concept of mantle cloaking, has been proposed [14], [15], [16], [17], [18], [34]. These cloaks are characterized by an average surface reactance and are based on the scattering cancellation of the dominant scattering mode using an ultra-thin metasurface. The mantle cloak metasurfaces seem to perform adequately at the microwave frequencies, however, due to the increase of losses in metallic elements, implementation of the mantle cloaks

The associate editor coordinating the review of this manuscript and approving it for publication was Bilal Khawaja.

become tedious at higher frequencies such as terahertz (THz) and infrared (IR). Considering this, graphene is regarded as a favorable material that can be utilized to design mantle cloaks at low-THz frequencies.

Graphene, an allotrope of carbon, gained popularity due to several attractive features like high tensile strength, stable thermal and mechanical properties, optical transparency, among others [35], [36], [37], [38], [39], [40], [41], [42], [43], [44], [45], [46], [47], [48]. To analyze graphene for its electromagnetic applications, it is necessary to study its complex surface conductivity model based on the Kubo formula [40]. The local surface conductivity is characterized by $\sigma_g(\omega, T, E_F, \tau)$,

$$\sigma_g(\omega) = -j\frac{e^2 k_B T}{\pi\hbar^2(\omega - j\tau^{-1})}\left[\frac{E_F}{k_B T} + 2\ln\left(1 + e^{-\frac{E_F}{k_B T}}\right)\right] - j\frac{e^2}{4\pi\hbar}\ln\left(\frac{2|E_F| - (\omega - j\tau^{-1})\hbar}{2|E_F| + (\omega - j\tau^{-1})\hbar}\right), \quad (1)$$

where ω is the radian frequency, T is the temperature ($T = 300$ K is used for the results obtained in this paper), E_F is the Fermi energy level, τ is the momentum relaxation time, $-e$ is the charge of an electron, $\hbar$ is the reduced Planck's constant, and k_B is the Boltzmann's constant. The first term in (1) represents the intra-band contribution, which is approximated using the condition $\hbar\omega \ll 2|E_F|$, and the second term represents the inter-band contribution. In the low-THz region (up-to 15 THz), the intra-band contribution dominates the inter-band contribution; nevertheless, both terms are included in our calculations.

A simple graphene monolayer is fashioned as a cloaking device in [41] and is demonstrated to enable scattering width (SW) reduction for dielectric objects in the THz spectrum. This design, however, is incapable of cloaking conducting objects due to the intrinsically inductive nature of graphene monolayer in the low-THz regime. Thus, a cloaking structure that employs graphene nano-patches (possessing a dual capacitive/inductive surface reactance) is introduced in [42]; both the dielectric and conducting objects are satisfactorily cloaked by properly tuning the surface impedance of the graphene metasurface. This idea is further extended to cloaking of the elliptical structures, which possess non-symmetric geometries, unlike circular configurations [44].

Now, according to the Kubo formula [40], the sheet impedance of graphene is inversely proportional to the carrier mobility and the Fermi energy level. Based on this fact, in order to achieve the desired functionality, most of the theoretical studies purposely assume a large mobility and/or high Fermi level to lower the sheet impedance of graphene. In these papers, graphene with extremely high mobility (more than 150, 000 $cm^2V^{-1}s^{-1}$, corresponding to $\tau = 1.5$ ps) is utilized. However, in practice, the carrier mobility of graphene cannot possess such high values owing to the impurities and defects that are introduced during the graphene growth and transfer. This poor carrier mobility is compensated by increasing the Fermi level of graphene ($E_F \approx 1$ eV), but this may disrupt graphene's band structure, compromising its tunability. To emphasize its importance, we present Fig. 1, wherein we show a comparison of SW plots, corresponding to the decrease in relaxation time (τ). The configuration (cloaked conducting cylinder; inset Fig. 1) and the geometrical dimensions have been referred from [42]; wherein graphene nano-patches are contrived as a cloaking device. It is demonstrated that as τ decreases, the magnitude of SW increases, which basically means that the cloaking action of the graphene nano-patches disappears (see the green and purple curves representing SW for $\tau = 200$ fs and $\tau = 20$ fs, respectively; the cloaking behavior is almost non-existent for such low values of relaxation times). Note that the relaxation time 'τ' is directly proportional to the carrier mobility of graphene, ergo, low mobility, practical graphene will be rendered unsuitable for cloaking purposes.

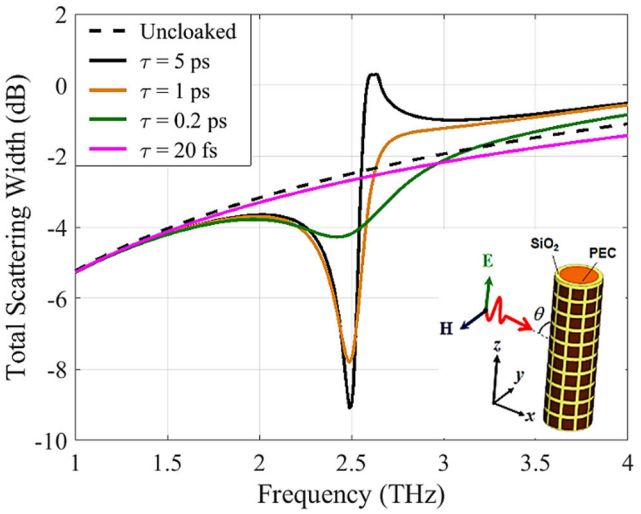

FIGURE 1. Scattering width (SW) versus frequency for a conducting cylinder covered by graphene nano-patches (inset) for decreasing values of the relaxation time 'τ'.

As a possible solution to these design challenges for practical graphene, a novel structure, positioning a graphene sheet on a specific metasurface substrate, is presented by X. Wang et al. [48]. This structure was modeled to show that a perfect and strongly tunable absorption is possible even in a very weakly doped graphene, without the strict requirements of the carrier mobility. In this paper, we make use of a graphene-metal metasurface structure inspired by the design in [48], to facilitate *cloaking* of PEC (perfect electrical conductor) cylindrical objects (circular and elliptical) and 2D PEC strip (as a degenerated elliptical cylinder), at low THz frequency. This metasurface design (see Fig. 2) employs a graphene monolayer with a very low carrier mobility, placed on a substrate embedded with periodic arrays of metallic patches. By wrapping this structure around the cylindrical objects, a considerable reduction in the SW is observed, thus illustrating the cloaking effect. We show that, by properly choosing the structural parameters, cloaking is perfectly possible even if the graphene sheet is very weakly doped.

Particularly, in the low mobility regime, we have designed two types of tunable cloaking devices; in the case of $\tau = 200$ fs (carrier mobility, $20,000$ $\mathrm{cm^2V^{-1}s^{-1}}$), our cloak structure enables tunability in the frequency of cloaking, whereas in the case of $\tau = 20$ fs (carrier mobility, $2,000$ $\mathrm{cm^2V^{-1}s^{-1}}$), the metasurface can operate as a switch between the cloaked and uncloaked functionalities.

The paper is organized as follows; Section II describes the proposed model for cloaking of PEC cylinders. In section III, we present the numerical results for the cloaked cylindrical objects at $\tau = 200$ fs and $\tau = 20$ fs. Section IV is allocated to the conclusions. A time dependence of the form $e^{j\omega t}$ is assumed and suppressed and all the results discussed in this paper pertain to a TM (transverse magnetic) polarized plane wave with normal incidence to the objects. The analytical results were calculated in the MATLAB software, whereas the full wave simulations were conducted with CST MWS [49].

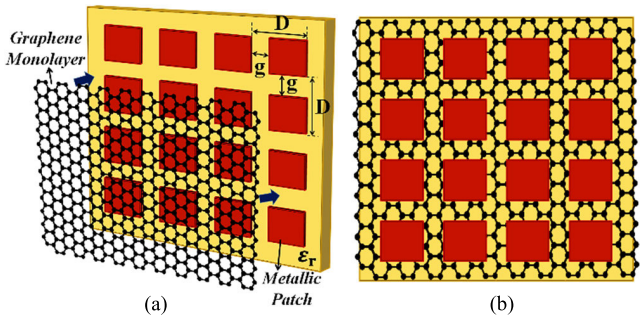

FIGURE 2. (a) Schematic and (b) physical structure for graphene-metal metasurface cloak.

II. DESIGN OF GRAPHENE-METAL METASURFACE

The schematic of the cloak designed with a graphene-metal metasurface is illustrated in Fig. 2(a) (the design is inspired from [48]). The figure shows an array of thin metallic subwavelength patches (period 'D' and gap 'g') placed on a dielectric substrate (permittivity 'ε_r'). Although the metallic patches in this paper are treated as perfect conductors, we also account for the Drude conductivity of the patches, which is dominant in the low THz regime (refer to the Appendix for the details). The graphene monolayer sheet is then transferred directly onto this metallic patch array. The metasurface, thus formed by the periodic square patch array and the substrate, plays the following important roles: realization of a capacitive component, together with inductive graphene to form a resonant cavity (high impedance surface), and reducing the effective shunt resistance of graphene. It is known that in order to cancel the dominant scattering mode of a conducting (PEC) object, capacitive surface reactance is desired and so, now our metasurface design should be able to effectively cloak the PEC cylindrical objects. The required capacitive reactance of the graphene-metal metasurface can be obtained by a proper selection of the gap size 'g', array periodicity 'D', and the Fermi energy level (E_F) of graphene.

Now, an interesting phenomenon occurs as a direct result of transferring graphene monolayer on the metallic patch arrays; in all the graphene-metal contact areas, graphene gets shorted by the highly conductive metallic patches (referred from [48]), resulting in the effective part of graphene which is not shorted, to resemble a fishnet-like pattern (see Fig. 2(b)). In other words, the surface of our cloak structure comprises of the square metallic patches along with the presence of the non-shorted part of the graphene in the gaps between the patches. As such, the equivalent circuit model of our proposed structure, effectually, is a parallel combination of the scaled-down impedance of 'patterned' graphene 'Z_p' ($Z_p = Z_g/p$; which can be expressed as a complex quantity: $R_p + jL_p$, where $Z_g = 1/\sigma_g$ is the surface impedance of graphene monolayer and p is called as the scaling factor [48], written as $p = (D-g)/g$), and the capacitive component 'Z_c', contributed by the periodically arranged metal patches, where $Z_c = 1/j\omega C_p$. For a normally incident plane wave, C_p is expressed as $C_p = \left((\varepsilon_r + 1)\,\varepsilon_0 D \ln\left[\csc\left(\pi g/2D\right)\right]\right)/\pi$ [50]. As a result, for the case of a uniform plane wave normally incident to the cloak surface, the surface impedance 'Z_s' of our proposed graphene-metal metasurface is given by a simple yet an accurate analytical expression:

$$Z_s = \frac{Z_p Z_c}{Z_p + Z_c}, \tag{2}$$

where the expression for Z_p and Z_c reads as,

$$Z_p = \left(\frac{\pi\hbar^2}{e^2 E_F}\frac{1}{\tau p}\right) + j\omega\left(\frac{\pi\hbar^2}{e^2 E_F}\frac{1}{p}\right), \tag{3}$$

and

$$Z_c = \frac{\pi}{j\omega\,(\varepsilon_r + 1)\,\varepsilon_0 D \ln\left[\csc\left(\frac{\pi g}{2D}\right)\right]}. \tag{4}$$

From (3),

$$R_p = \pi\hbar^2 \Big/ \left(e^2 E_F \tau p\right)$$

and

$$L_p = \pi\hbar^2 \Big/ \left(e^2 E_F p\right).$$

Thus, the total surface impedance of the metasurface is

$$Z_s = \frac{R_p}{\left(1-\omega^2 L_p C_p\right)^2 + \left(\omega C_p R_p\right)^2} + j\omega\frac{L_p\left(1-\omega^2 L_p C_p\right) - C_p R_p^2}{\left(1-\omega^2 L_p C_p\right)^2 + \left(\omega C_p R_p\right)^2}. \tag{5}$$

It is interesting to observe that this particular design gives rise to the parallel resonance condition of the metasurface. At the lower frequencies, the surface reactance of the metasurface is inductive in nature; this inductive reactance dominates until the resonance frequency is reached, where, the impedance is at its maximum. As the frequency goes above resonance, the metasurface starts to exhibit capacitive behavior and the capacitive reactance dominates beyond this point (refer to Fig. 3, wherein a comparison between the surface reactance

plots for a simple graphene monolayer and the graphene-metal metasurface is shown for increasing values of the Fermi energy E_F). The structural parameters used for the plots in Fig. 3 are given in subsection A of section III for the case of $\tau = 200$ fs. In Fig. 3, we can see that the surface reactance of the graphene monolayer is always inductive at low-THz frequencies (observe the dashed curves), whereas the surface reactance of the graphene-metal metasurface goes from being inductive to capacitive, as it experiences the parallel resonance (observe the solid curves). This property of the metasurface structure (specifically its capacitive behavior) motivated us to study its cloaking property in the case of conducting cylinders. We should comment here that, the transition from inductive to capacitive surface impedance of the structure is tunable with the Fermi energy E_F and can also be controlled by varying the period D and gap size g.

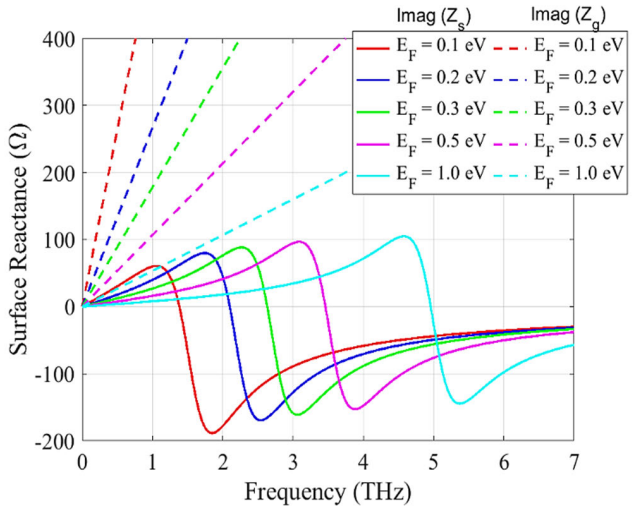

FIGURE 3. Surface reactance plots for the graphene monolayer (dashed curves) and the graphene-metal metasurface (solid curves) at $\tau = 200$ fs for increasing values of Fermi energy E_F.

Additionally, we have presented the behavior of the surface resistance of the metasurface (Fig. 4(a)) in comparison to that of the graphene monolayer (Fig. 4(b)) for $\tau = 200$ fs. From Fig. 4(a), we see that resistance of the metasurface increases with frequency until the parallel resonance condition is met, at which point, it is maximum. After the resonance point, the resistance goes on decreasing with frequency. By comparing Fig. 4(a) and (b), we conclude that the graphene metasurface design greatly reduces the surface impedance.

In this paper, firstly we consider an infinite PEC circular cylinder enclosed by a conformal graphene-metal metasurface cloak, impinged by a normally incident TM polarized plane wave (see Fig. 5). For this case, the mathematical formulation to analyze the scattering problem is based on the Lorenz–Mie scattering theory [51], [52], which gives the expression for the total scattering width, as a quantitative measure of the overall visibility of the object. The incident and the scattered electric and magnetic fields of the plane wave may be expanded in terms of cylindrical harmonics with complex scattering coefficients [53], [54], which can be determined by imposing boundary conditions at the two radial interfaces (i.e., surface of the PEC cylinder and the graphene-metal metasurface). We should remark that, while the tangential electric fields are continuous across the metasurface, the use of high impedance surface causes discontinuity of the tangential magnetic field components.

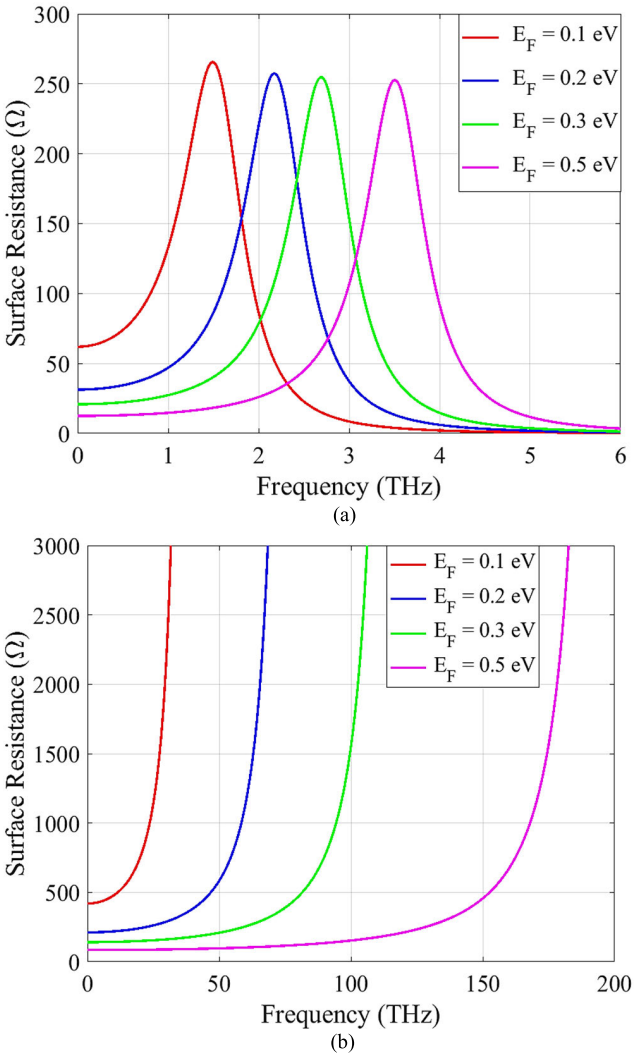

FIGURE 4. Surface resistance plots for (a) graphene-metal metasurface, and (b) graphene monolayer at $\tau = 200$ fs for increasing values of Fermi energy E_F.

Next, we consider the case of an infinitely long PEC elliptical cylinder, cloaked by the given graphene-metal metasurface (Fig. 11) and a 2D PEC strip (modeled as a degenerated ellipse) also enclosed by the metasurface (Fig. 15). The analytical formulation of the scattering problem for these instances is based on the method of separation of variables in order to solve the 2D wave equation in the elliptical coordinates, and subsequently, solving the well-known angular and radial Mathieu equations, as depicted in [44] and [55]. This results in a linear system of equations for the unknown amplitude of complex coefficients of the scattered field, which is

solved numerically with the focus on the dominant scattering mode.

III. RESULTS AND DISCUSSIONS

In the present section, we take into consideration different cylindrical objects (circular and elliptical) as well as a 2D PEC strip (which is modeled as a degenerated ellipse) cloaked by the conformal graphene-metal metasurfaces. We demonstrate the applicability and effectiveness of the proposed cloaking structures by presenting several numerical results of our analytical approach. We have also provided comparison and confirmation for these analytical results using full-wave simulations performed with CST Microwave Studio [48].

A. CLOAKING OF CIRCULAR CYLINDERS

We take into consideration an infinitely long circular PEC cylinder with radius a. The respective designed metasurface is wrapped around this conducting cylinder concentrically, with the intention to make it 'invisible' (i.e., to bring about reduction in the SW of the PEC cylinder) to a normally incident TM polarized uniform plane wave. The dielectric substrate with relative permittivity ε_r, used as a part of our metasurface design, also plays the role of a spacer over the conducting cylinder, thereby avoiding an electrical short. The radius of this circular dielectric spacer is a_c. Refer to Fig. 5 for the schematic configuration and the cross-sectional view of the structure.

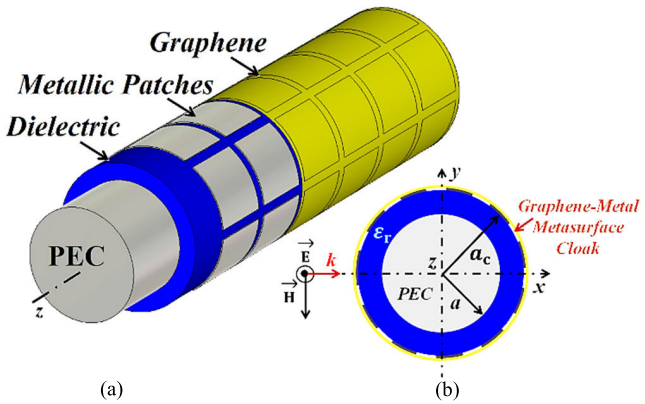

FIGURE 5. (a) Schematic and (b) cross-sectional view of a circular PEC cylinder cloaked with the graphene-metal metasurface.

The quasi-static approximate expression for optimum surface reactance X_{opt}, to effectively cloak a conducting cylinder covered by a thin spacer (permittivity ε_r) under TM-polarized illumination, is obtained by generalizing the results in [5]:

$$X_{opt} \cong \omega\mu_0 a \frac{\gamma^2 - 1}{\gamma\left(\gamma^2 + 1\right)}, \tag{6}$$

where μ_0 is the permeability of the free space, and $\gamma = a/a_c$. Here, X_{opt} is an analytically extracted expression for the surface reactance, under the assumption that the amplitude of the coefficient corresponding to the dominant scattering mode is required to be zero (essentially ensuring that there is no scattering of the dominant mode). Also, we would like to mention that the simple closed form expression for X_{opt} is obtained for a small-argument approximation of the Hankel and Bessel functions. Since this expression is frequency dependent, we have plotted the curve for X_{opt} with respect to frequency (see Fig. 7(b) and 10(b)) and an intersection point on this curve should give the required value of the surface reactance that will ensure zero scattering of the dominant mode, thereby facilitating the cloaking effect. As mentioned before, the graphene-metal metasurface in Fig. 2(b) has a dual inductive/capacitive nature. Since we are concerned with cloaking of the conducting cylinders, we concentrate on bringing out the capacitive nature of the metasurface. This is possible by appropriate selection of the metasurface parameters, effectually balancing the intrinsic kinetic inductance of graphene with the negative reactance provided by the capacitive metallic patches. We demonstrate the cloaking effect using low-mobility graphene, specifically corresponding to the relaxation times of $\tau = 200$ fs and $\tau = 20$ fs, employing low Fermi energy values (as low as $E_F = 0.1$ eV).

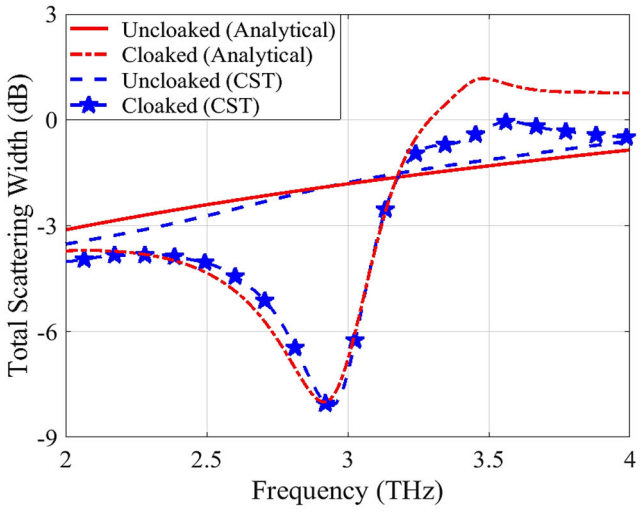

FIGURE 6. Frequency variation of the total SW for a circular PEC cylinder cloaked by graphene-metal metasurface ($\tau = 200$ fs and $E_F = 0.1$ eV).

For the case of $\tau = 200$ fs (mobility 20, 000 $cm^2V^{-1}s^{-1}$), following parameters were chosen for the metasurface cloak design: $a_c = 13\ \mu$m, $a = 10\ \mu$m, $\varepsilon_r = 12$, $g = 1.75\ \mu$m, $D = 13.6136\ \mu$m, and $E_F = 0.1$ eV. It is evident from Fig. 6 that there is a considerable decrease in the SW for the cloaked circular cylinder as compared to the uncloaked case. We have also provided validation for the analytical results in Fig. 6 using the full-wave numerical simulations obtained with CST. The magnitude of the total SW reduces by approximately 6.5 dB for both analytical and simulation results at the frequency 2.95 THz. In addition to this, we have also illustrated tunability in the frequency of cloaking at $\tau = 200$ fs (the design specifications indicated above are used here as well).

By changing the value of Fermi energy E_F, we achieve reduction in the total SW at different frequencies, as shown in Fig. 7(a). We further relate these plots to the frequency dispersion of surface reactance in Fig. 7(b), wherein surface reactance of the graphene-metal metasurface is plotted for the increasing values of Fermi energy E_F. Along with this, the optimal surface reactance X_{opt} calculated using (6), is also plotted (shown by dotted black curve).

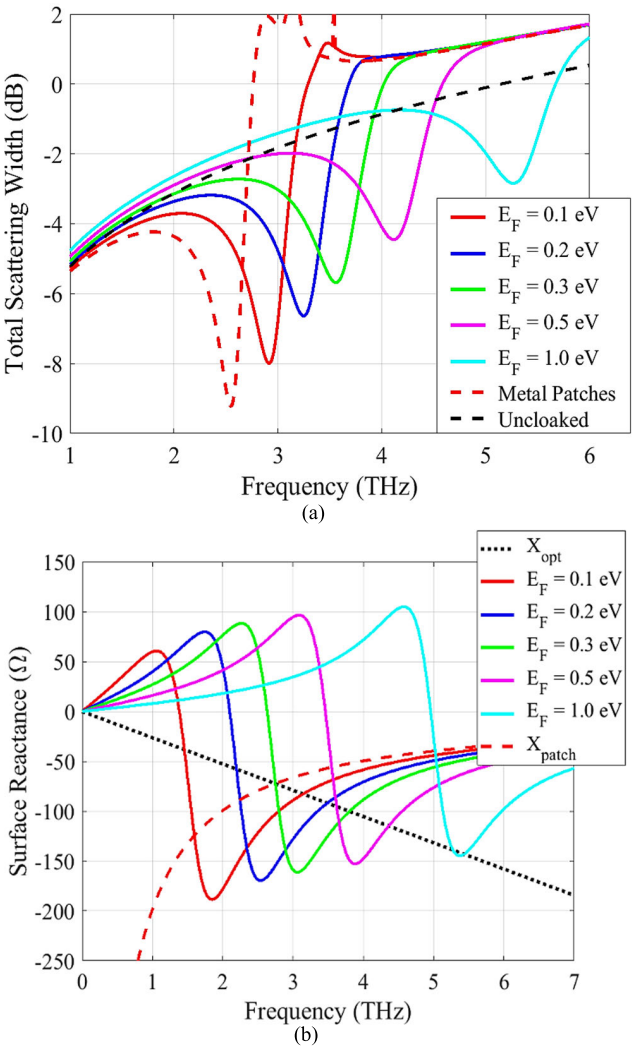

FIGURE 7. (a) SW versus frequency for a cloaked circular PEC cylinder, showing tunability in cloaking frequency, and (b) frequency dispersion of the surface reactance for different Fermi energy (E_F).

Through Fig. 7(b), we attempt to exhibit that it is possible to tune the surface reactance of the metasurface such that the capacitive region of the curve intersects the required value on the X_{opt} curve, in order to target a desired cloaking frequency. We would like to draw your attention to Fig. 7(b), wherein two intersection points are observed for every surface reactance plot (solid colored plots) on the X_{opt} curve (dotted black curve). However, we are not interested in the first intersection points since they highlight the intersection of the 'resonance' region of the surface reactance (of the graphene-metal metasurface) with the X_{opt} curve, and consequently, do not contribute towards cloaking of the cylindrical objects. We are more interested in the second intersection points because these points emphasize the intersection of the 'capacitive' region of the surface reactance plots with the X_{opt} curve. These junction points are crucial to our design as they provide the capacitive surface reactance values (of the metasurface) necessary to achieve the cancellation of the dominant scattering mode of the conducting (inductive) cylinder. Another important role that these second intersection points play is that they indicate the approximate cloaking frequency of the design at a particular Fermi energy level. For instance, from Fig. 7(b), for $E_F = 0.1$ eV, the junction point of the capacitive part of the plot with the X_{opt} curve is seen at the frequency 3.08 THz (the value of X_{opt} at this intersection point is $-83.29\ \Omega$). Now, observe Fig. 7(a); for $E_F = 0.1$ eV, the minimum of the total scattering width (cloaking effect) is seen at the frequency 2.95 THz. Similarly, for $E_F = 0.2$ eV in Fig. 7(b), the intersection occurs at 3.42 THz (the value of X_{opt} is $-91.77\ \Omega$), and from Fig. 7(a), for $E_F = 0.2$ eV, cloaking effect is seen at the frequency 3.29 THz. Similar observations can be made for the plots at the remaining Fermi energy levels. Note that in Fig. 7, a supplementary dashed red curve is plotted to observe the behavior of metallic patches, in the absence of graphene monolayer. This serves as a comparison point between the inherent capacitive nature of the metallic patches and the induced capacitive action of the graphene-metal metasurface. We should mention here that in Fig. 7(a), the magnitude of scattering width is seen to increase with the increase in Fermi level E_F, indicating that there is an apparent deterioration in the cloaking performance. To explain this peculiarity, we compare Fig. 7(a) and Fig. 4(a). It is evident that at $E_F = 0.1$ eV, cloaking frequency is 2.95 THz (Fig. 7(a)), and the surface resistance at this frequency is around 9.8 Ω (Fig. 4(a)). Next, at $E_F = 0.2$ eV, the frequency of cloaking is 3.29 THz (Fig. 7(a)), and the surface resistance at this frequency is found to be approximately 21 Ω (Fig. 4(a)). Similarly, at $E_F = 0.3$ eV, cloaking is observed at 3.56 THz (Fig. 7(a)) and the surface resistance at this frequency is around 35 Ω (Fig. 4(a)), and so on. Hence, we can say that as the Fermi level increases, there is an increment in the surface resistance values at the cloaking frequency of the metasurface design. Accordingly, we attribute this behavior to the increase in the ohmic losses at the cloaking frequencies, when the Fermi energy levels are increased. Nevertheless, even at the higher Fermi levels (especially at $E_F = 1$ eV), the cloaking action of the metasurface design does not completely deteriorate; the cloak design manages to provide enough reduction in the scattering width as compared to the uncloaked case. Moreover, we also exhibit the snapshots of the electric field distribution for infinitely long, uncloaked and cloaked circular PEC cylinder, at the cloaking frequency 2.95 THz, in Fig. 8 to further exemplify the cloaking functionality of our design. It can be clearly seen that the wave fronts of the electric field are strongly perturbed in the absence of the cloak, which are then restored

by wrapping the suitable graphene metasurface around the cylindrical object.

The exciting cloaking feature of our metasurface design is also demonstrated at an extremely low mobility value of $2,000\ \mathrm{cm^2V^{-1}s^{-1}}$, corresponding to the relaxation time $\tau = 20$ fs. The design parameters are: $a_c = 14\ \mu$m, $a = 10\ \mu$m, $\varepsilon_r = 12$, $D = 10.99\ \mu$m, $g = 1.75\ \mu$m, and $E_F = 0.1$ eV. It is manifested in Fig. 9 that the metasurface leads to a substantial suppression of the total SW at the frequency 2.5 THz and the full-wave simulation results agree well with the analytical results. The SW decreases from -2.3 dB (uncloaked case) to -8.8 dB (cloaked case) for the analytical results, and for the CST simulation results, the SW drops down from -2.2 dB (uncloaked case) to -9 dB (cloaked case).

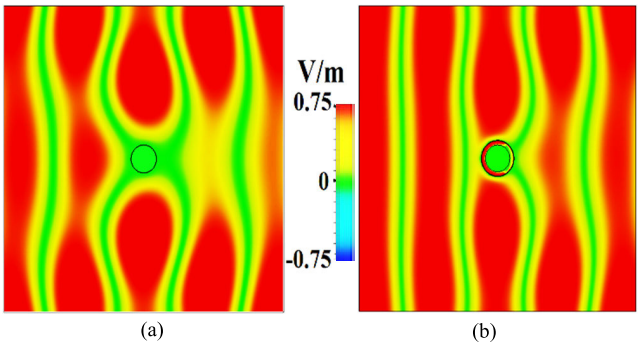

FIGURE 8. Frequency variation of the total SW for a circular PEC cylinder cloaked by graphene-metal metasurface ($\tau = 20$ fs and $E_F = 0.1$ eV).

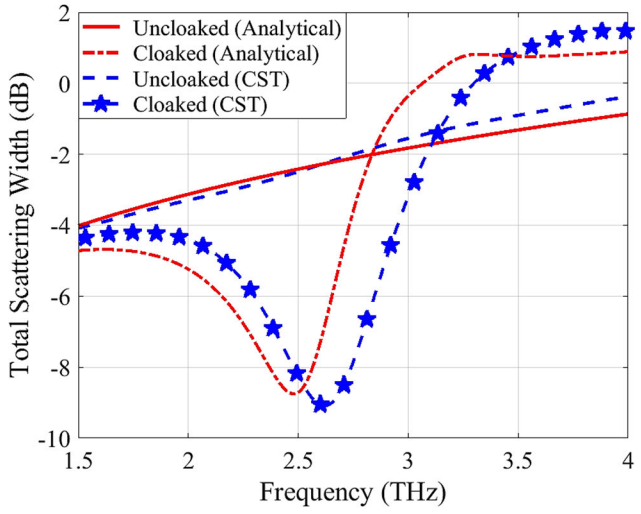

FIGURE 9. Snapshots of the electric field distribution for (a) uncloaked and (b) cloaked circular cylinder impinged by a TM-polarized plane wave at normal incidence for $\tau = 200$ fs.

Now, it was found that the surface resistance values of the graphene-metal metasurface are higher at the cloaking frequencies for the low quality, highly lossy graphene (having low mobility values); and that at very low mobilities, the value of resistance further increases with increase in the Fermi energy E_F. While this hampers the ability of the metasurface to act as a frequency-tunable cloaking device, the metasurface however, proves to be an excellent switch between the cloaked and uncloaked functionalities, at extremely low mobility values. It is apparent from Fig. 10(a) that the magnitude of SW goes on increasing with increasing E_F values, which means that cloaking behavior of the metasurface gradually tends to disappear, and for $E_F > 0.5$ eV, the metasurface no longer functions as a 'cloak'.

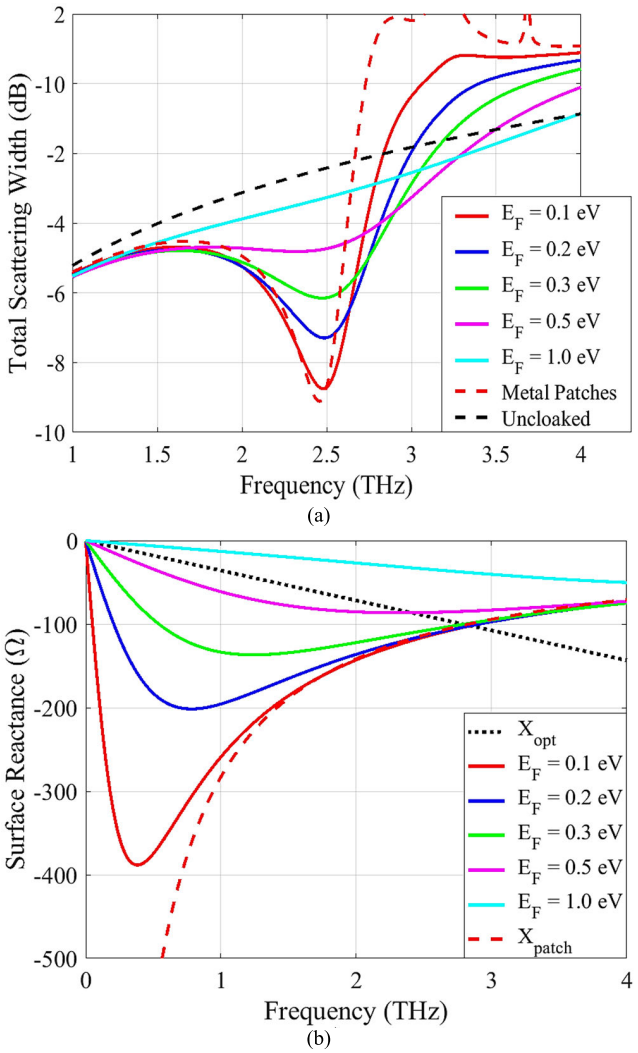

FIGURE 10. SW versus frequency for a cloaked circular PEC cylinder, showing tunability in magnitude of cloaking, and (b) frequency dispersion of the surface reactance for different Fermi energy (E_F).

The frequency dispersion plot for the surface reactance of graphene-metal metasurface along with the optimal surface reactance curve X_{opt} for effective cloaking of a conducting cylinder (dotted black curve) is presented in Fig. 10(b). The dashed red curves in Fig. 10 denote the plots for the performance of metallic patches in absence of the graphene monolayer. It is interesting to see that the behavior of graphene-metal metasurface at $E_F = 0.1$ eV (refer to the solid red curve in Fig. 10) is very much similar to that of the metallic patches, when low quality graphene (having

very low carrier mobility, in this case 2, 000 $\text{cm}^2\text{V}^{-1}\text{s}^{-1}$) is employed. However, our graphene-metal metasurface adds on the 'cloaking tunability' feature to the cylindrical object that is encompassed by it.

B. CLOAKING OF ELLIPTICAL CYLINDERS AND 2D PEC STRIP

1) ELLIPTICAL CYLINDERS

Here, we show that the same metasurface design that is used to cloak circular cylinders, can now be adopted to bring about cloaking of the elliptical PEC cylinders. Consider a long infinite length of a conducting elliptical rod (semi-major axis 'a_0' and semi-minor axis 'b_0'). The confocal, elliptically shaped graphene-metal metasurface is wrapped around this rod to achieve scattering reduction at a desired frequency (refer to Fig. 11 for the schematic configuration).

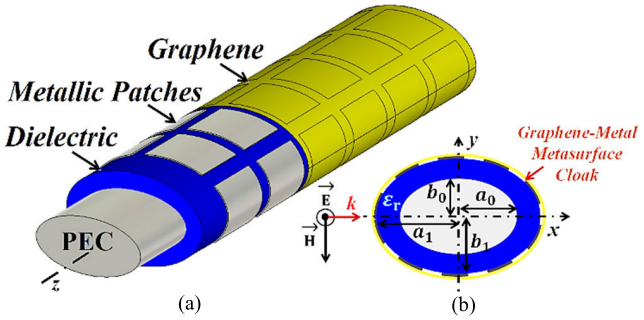

FIGURE 11. Schematic and (b) cross-sectional view of the elliptical PEC cylinder cloaked with the graphene-metal metasurface.

For elliptical cylinders as well, we demonstrate that by appropriate selection of the structural parameters for the metasurface cloak, it is possible to make the conducting ellipse 'invisible' to the normally incident uniform TM polarized plane wave. Similar to previous subsection, we show the cloaking effect using low-mobility, low quality practical graphene. In this regard, for the relaxation time of $\tau = 200$ fs (mobility 20, 000 $\text{cm}^2\text{V}^{-1}\text{s}^{-1}$), following structural dimensions were selected: $a_0 = 10.04\ \mu$m, $b_0 = 6.67\ \mu$m, $a_1 = 12.5\ \mu$m, $b_1 = 10\ \mu$m, $\varepsilon_r = 10$, $D = 14.18\ \mu$m, $g = 2.25\ \mu$m and $E_F = 0.1$ eV. As illustrated in Fig. 10(a), there is a substantial reduction in the SW for the cloaked elliptical cylinder with reference to the uncloaked case at the frequency 3.3 THz. The full-wave numerical simulation results, obtained with CST, are provided in Fig. 12(a), to verify the analytical results. For analytical results, a difference of 10 dB, whereas for simulation results with CST, a difference of 8.9 dB is recorded between the uncloaked and cloaked conditions at 3.3 THz. Furthermore, we have shown the frequency tunability feature of our cloak structure in Fig. 12(b). By changing the Fermi energy E_F, we can achieve reduction of the total SW at different frequencies.

In addition to this, to visualize the cloaking effect of the metasurface design, we present the snapshots of the electric field distribution for the uncloaked and cloaked elliptical PEC cylinder for $\tau = 200$ fs, at the cloaking frequency 3.3 THz, in Fig. 13. This further corroborates the successful cloaking action of our design. From Fig. 13, we can clearly see the strong perturbations in the wave fronts of the electric field, in the absence of the cloak, which are then restored by wrapping the suitable graphene metasurface around the elliptical PEC object.

Similarly, we present the numerical results for $\tau = 20$ fs (mobility 2, 000 $\text{cm}^2\text{V}^{-1}\text{s}^{-1}$) in Fig. 14. The dimensions used for this case are the same as that of$\tau = 200$ fs. In Fig. 14(a), a noticeable decrease in the SW is observed at the frequency 3 THz and the analytical plots are validated by the full wave numerical plots (obtained with CST). A scattering reduction of approximately 9 dB is noted for both analytical and simulation results at 3 THz. For this extremely low mobility regime, we have also shown the tunability in the magnitude of cloaking in Fig. 14(b). As the Fermi energy level E_F increases, the cloaking action of the metasurface structure starts to disappear (this is evident from the increase in the magnitude of SW). Thus, for $\tau = 20$ fs, the metasurface acts as a tunable switch between the cloaked and uncloaked functionality.

2) 2D PEC STRIP

We finally present a special case of 2D metallic (PEC) strip, which is modeled as a degenerated metallic elliptical cylinder ($b_0 = 0$) and again, the same metasurface construct is utilized to facilitate cloaking of this 2D strip. To obtain the optimum scattering reduction, we cloak the metallic strip by placing the focal points of the elliptically shaped graphene metasurface at the edges of the strip. Fig. 15 shows the schematic for the cloaked configuration.

We proceed to show that excellent cloaking action is observed for the 2D strip, illuminated by a normally incident uniform TM polarized plane wave, when it is enclosed by the graphene-metal metasurface structure. As per usual, proper selection of the design parameter values is necessary to bring about the desired cloaking effect. Similar to the discussions in the previous sections, we endeavor to facilitate cloaking of the 2D strip using a very practical graphene (characterized by low mobility values), with a low Fermi energy level (particularly at $E_F = 0.1$ eV). As such, we make use of graphene with $\tau = 200$ fs and 20 fs, and design our cloaking structure with the following dimensions: $a_0 = 7.5\ \mu$m, $b_0 = 0\ \mu$m, $a_1 = 10.04\ \mu$m, $b_1 = 6.67\ \mu$m, $D = 10.6\ \mu$m, $g = 2.75\ \mu$m, $\varepsilon_r = 8$ and $E_F = 0.1$ eV.

To substantiate our claim, we present the plots for frequency dispersion of SW in Fig. 16 (a) and (b), for the cases of $\tau = 200$ fs and 20 fs, respectively. For both of these instances, a substantial amount of reduction is observed in the magnitude of total SW for the cloaked 2D strip. The full wave numerical simulation results in these plots serve to validate the analytical results. The magnitude of SW decreases by 16.5 dB and 12 dB for the analytical and the full-wave simulation results, respectively, at 3.3 THz for $\tau = 200$ fs (see Fig. 16(a)).

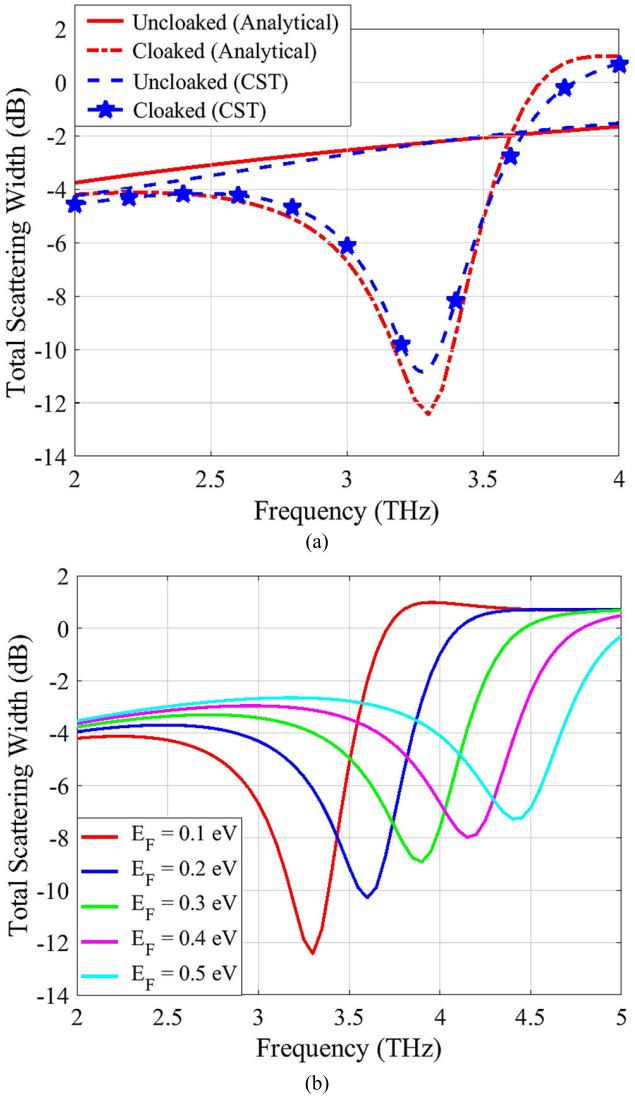

FIGURE 12. (a) Frequency dispersion of the total SW and (b) SW versus frequency, showing tunability in cloaking frequency for an elliptical PEC cylinder cloaked by graphene-metal metasurface for $\tau = 200$ fs.

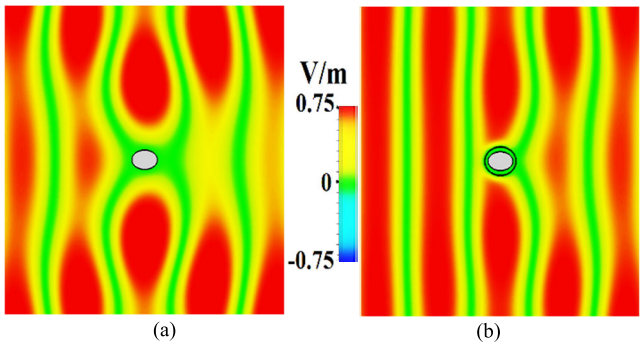

FIGURE 13. Snapshots of the electric field distribution for (a) uncloaked, and (b) cloaked elliptical cylinder impinged by a TM-polarized plane wave at normal incidence for $\tau = 200$ fs.

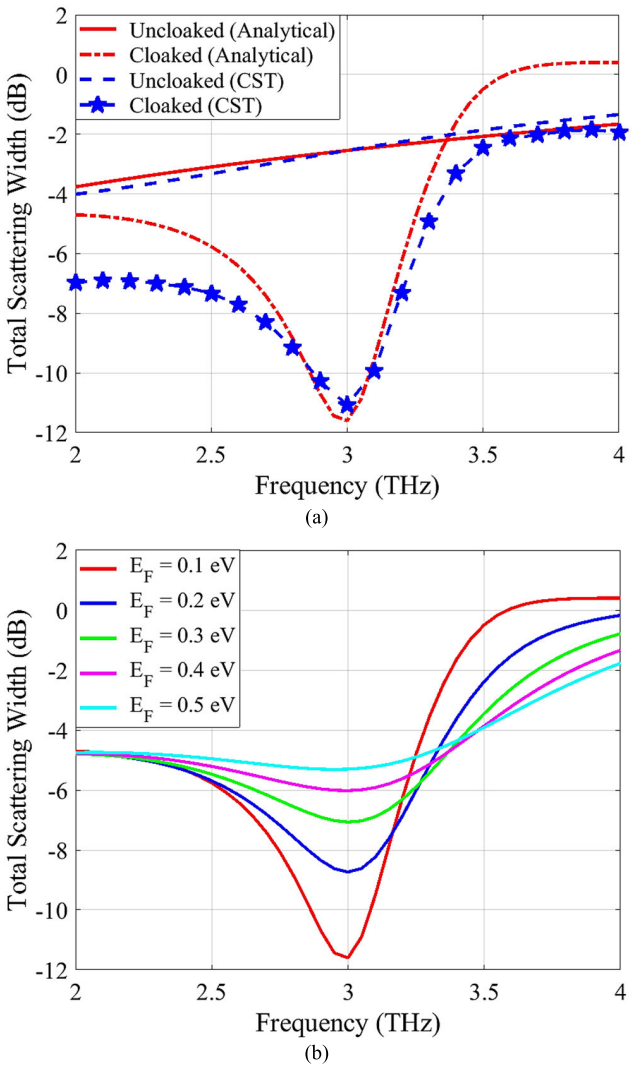

FIGURE 14. Frequency dispersion of the total SW and (b) SW versus frequency, showing tunability in magnitude of cloaking for an elliptical PEC cylinder cloaked by graphene-metal metasurface for $\tau = 20$ fs.

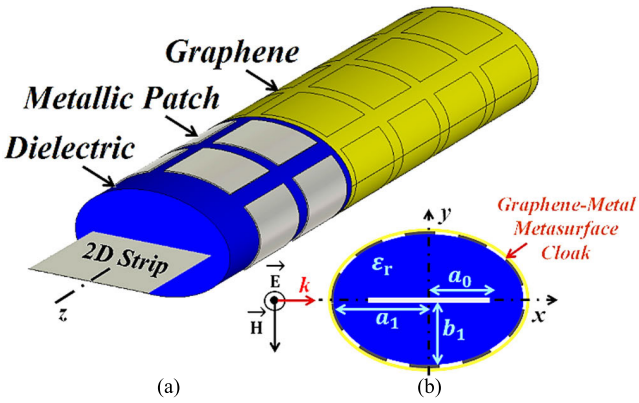

FIGURE 15. Schematic and (b) cross-sectional view of the 2D PEC strip, cloaked with the graphene-metal metasurface.

Similarly, for $\tau = 20$ fs, a reduction of 13 dB and 10 dB in the total SW is noted for analytical and simulation results, respectively, at 3 THz. We should comment here that the numerical results demonstrating the frequency tunability

feature at $\tau = 200$ fs, and the switchable cloaking action at $\tau = 20$ fs, for the cloaked 2D strip are not provided to avoid repetitiveness; however the metasurface cloak is perfectly capable of achieving the said tunability features even for the case of 2D PEC strip.

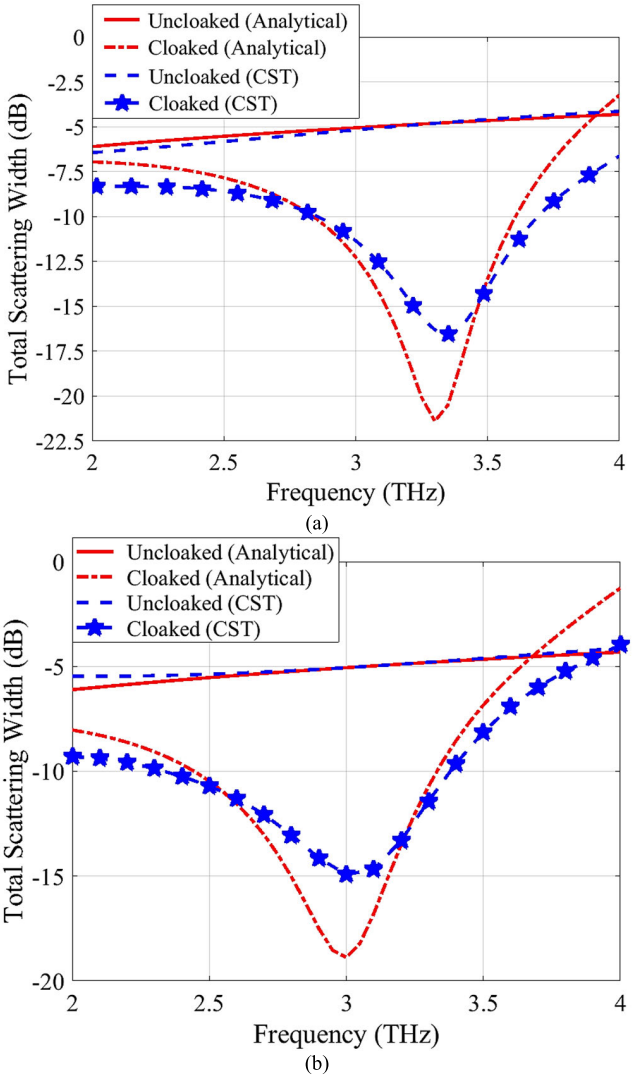

FIGURE 16. Frequency variation of the total SW for (a) $\tau = 200$ fs and (b) $\tau = 20$ fs for a 2D PEC strip cloaked by the graphene-metal metasurface.

To give a visual representation of the cloaking effect of the metasurface design on the 2D strip, the snapshots depicting electric field distribution for the uncloaked and cloaked PEC strip, is presented for $\tau = 200$ fs, at the cloaking frequency 3 THz, in Fig. 17.

The electrical field distribution snapshots correspond to a propagating plane wave incident normally to the structure (see Fig. 15). This substantiates the successful cloaking action of our metasurface design. In Fig. 15, we can clearly see the strong perturbations in the wave fronts of the electric field, in the absence of the cloak, which are then restored

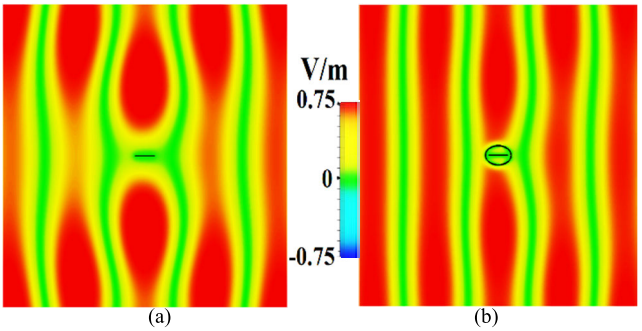

FIGURE 17. Snapshots of the electric field distribution for (a) uncloaked and (b) cloaked 2D PEC strip impinged by a TM-polarized plane wave at normal incidence for $\tau = 200$ fs.

by encasing 2D PEC strip by the specifically engineered graphene-metal metasurface.

IV. CONCLUSION

In this paper, we have presented a unique metasurface construct for cloaking of circular, elliptical PEC cylinders, and also 2D PEC strip, as a special case. The design configuration involves the use of graphene-metal metasurface cloaks, which adopts the mantle cloaking approach to facilitate reduction in the total scattering width of the conducting objects. In addition to this, we also illustrate the tuning capabilities of this metasurface design. Particularly, we demonstrate the cloaking effect even with the use of low-quality graphene, using very low Fermi energy values, which exemplifies the potency of our design for practical applications.

APPENDIX

To gain an insight into the Drude conductivity of the metallic patches, we consider the patches to be characterized by a complex surface conductivity σ^{DRUDE} (Sm^{-1}),

$$\sigma^{\mathrm{DRUDE}} = \frac{\omega_{\mathrm{p}}^2 \tau_{\mathrm{m}} \varepsilon_0}{1 + j\omega\tau_{\mathrm{m}}}, \tag{7}$$

where ω_{p} is the plasma frequency, ω is the radian frequency, $\tau_{\mathrm{m}} = 1/\Gamma_{\mathrm{m}}$ is the phenomenological scattering time for the metal, and ε_0 is the permittivity of free space. Thus, for the metallic patch array depicted in Fig. 2, the patch array surface impedance Z_{m} [43] is now given as,

$$Z_{\mathrm{m}} = \frac{D}{(D-g)\,\sigma^{\mathrm{DRUDE}} t} + \frac{1}{j\omega C_{\mathrm{p}}}, \tag{8}$$

where D is the period, g is the gap size, t is the thickness of the metallic patches, and $Z_{\mathrm{c}} = 1/(j\omega C_{\mathrm{p}})$ is the capacitive impedance associated with the patch geometry ($C_{\mathrm{p}} = \left((\varepsilon_{\mathrm{r}}+1)\,\varepsilon_0 D \ln\left[\csc\left(\pi g/2D\right)\right]\right)/\pi$) [50].

Now, we consider gold metallic patches with the following parameters: plasma frequency $\omega_{\mathrm{p}} = 1.36 \times 10^{16}$ rad/s and scattering rate $\Gamma_{\mathrm{m}} = 3.333 \times 10^{13}$ rad/s. As an example, at 3 THz, using the above parameters, the Drude conductivity for gold patches is calculated to be $\sigma^{\mathrm{DRUDE}} = \left(3.7226 \times 10^7\right) - j\left(2.1051 \times 10^7\right)$ Sm $^{-1}$.

Let the first term in (2) be denoted as 'Z_D'; therefore $Z_D = D/\left[(D-g)\,\sigma^{\mathrm{DRUDE}}t\right]$. For $D = 10.99\ \mu$m, $g = 1.75\ \mu$m and $t = 75$ nm, we calculate Z_D to be $Z_D = (0.3228 + j0.1825)\ \Omega$.

Next, we determine the value of the second term in (2), i.e. 'Z_c'. For $D = 10.99\ \mu$m, $g = 1.75\ \mu$m and $\varepsilon_r = 12$, we obtain the value of Z_c as $Z_c = j\,(-94.2812)\,\Omega$. Hence, at 3 THz, the surface impedance of the gold metallic patches 'Z_m' as depicted in (2) calculates to be $Z_m = (0.3228) - j\,(94.0987)\ \Omega$. As such, the surface impedance Z_m consists of a very small real resistance and a capacitive reactance. It is apparent that the impedance value of 'Z_D' is insignificant when compared to the value of 'Z_c', clearly indicating that the geometric patch capacitance dominates the weakly inductive reactance contributed by the Drude conductivity. This is typical for metallic patches in the low THz range of frequencies. Consequently, for the sake of simplicity, we neglect the contribution from the Drude conductivity and treat the metallic patches as perfect conducting materials in this paper.

REFERENCES

[1] J. B. Pendry, D. Schurig, and D. R. Smith, "Controlling electromagnetic fields," *Science*, vol. 312, no. 5781, pp. 1780–1782, May 2006, doi: 10.1126/science.1125907.

[2] H. Chen, C. T. Chan, and P. Sheng, "Transformation optics and metamaterials," *Nature Mater.*, vol. 9, no. 5, pp. 387–396, May 2010, doi: 10.1038/nmat2743.

[3] A. Vakil and N. Engheta, "Transformation optics using graphene," *Science*, vol. 332, no. 6035, pp. 1291–1294, 2011, doi: 10.1126/science.1202691.

[4] J. Li and J. B. Pendry, "Hiding under the carpet: A new strategy for cloaking," *Phys. Rev. Lett.*, vol. 101, no. 20, pp. 1–11, Nov. 2008.

[5] D. Schurig, J. Mock, J. Justice, S. Cummer, J. Pendry, A. Starr, and D. Smith, "Metamaterial electromagnetic cloak at microwave frequencies," *Science*, vol. 314, no. 5801, pp. 977–980, Oct. 2006.

[6] P. Sheng, "Waves on the horizon," *Science*, vol. 313, no. 5792, pp. 1399–1400, Sep. 2006.

[7] Z. Ruan, M. Yan, C. W. Neff, and M. Qiu, "Ideal cylindrical cloak: Perfect but sensitive to tiny perturbations," *Phys. Rev. Lett.*, vol. 99, no. 11, Sep. 2007, Art. no. 113903.

[8] A. Alù and N. Engheta, "Achieving transparency with plasmonic and metamaterial coatings," *Phys. Rev. E, Stat. Phys. Plasmas Fluids Relat. Interdiscip. Top.*, vol. 72, no. 1, Jul. 2005, Art. no. 016623, doi: 10.1103/PhysRevE.72.016623.

[9] A. Alù and N. Engheta, "Cloaking and transparency for collections of particles with metamaterial and plasmonic covers," *Opt. Exp.*, vol. 15, no. 12, pp. 7578–7590, Jun. 2007, doi: 10.1364/OE.15.007578.

[10] B. Edwards, A. Alù, M. G. Silveirinha, and N. Engheta, "Experimental verification of plasmonic cloaking at microwave frequencies with metamaterials," *Phys. Rev. Lett.*, vol. 103, no. 15, Oct. 2009, Art. no. 153901, doi: 10.1103/PHYSREVLETT.103.153901.

[11] P. Alitalo, O. Luukkonen, L. Jylha, J. Venermo, and S. A. Tretyakov, "Transmission-line networks cloaking objects from electromagnetic fields," *IEEE Trans. Antennas. Propag.*, vol. 56, no. 2, pp. 416–424, Feb. 2008, doi: 10.1109/TAP.2007.915469.

[12] S. Tretyakov, P. Alitalo, O. Luukkonen, and C. Simovski, "Broadband electromagnetic cloaking of long cylindrical objects," *Phys. Rev. Lett.*, vol. 103, no. 10, Sep. 2009, Art. no. 103905.

[13] P. Alitalo, J. Vehmas, and S. Tretyakov, "Reduction of antenna blockage with a transmission-line cloak," in *Proc. Eur. Conf. Antennas Propag.*, Rome, Italy, Apr. 2011, pp. 2399–2402.

[14] A. Alù, "Mantle cloak: Invisibility induced by a surface," *Phys. Rev. B, Condens. Matter*, vol. 80, no. 24, Dec. 2009, Art. no. 245115, doi: 10.1103/PhysRevB.80.245115.

[15] P.-Y. Chen and A. Alù, "Mantle cloaking using thin patterned metasurfaces," *Phys. Rev. B, Condens. Matter*, vol. 84, no. 20, Nov. 2011, Art. no. 205110, doi: 10.1103/PhysRevB.84.205110.

[16] P. Chen, F. Monticone, and A. Alù, "Suppressing the electromagnetic scattering with a helical mantle cloak," *IEEE Antennas Wireless Propag. Lett.*, vol. 10, pp. 1598–1601, 2011.

[17] Y. R. Padooru, A. B. Yakovlev, P.-Y. Chen, and A. Alù, "Analytical modeling of conformal mantle cloaks for cylindrical objects using subwavelength printed and slotted arrays," *J. Appl. Phys.*, vol. 112, no. 3, Aug. 2012, Art. no. 034907, doi: 10.1063/1.4745888.

[18] P.-Y. Chen, C. Argyropoulos, and A. Alù, "Broadening the cloaking bandwidth with non-foster metasurfaces," *Phys. Rev. Lett.*, vol. 111, no. 23, Dec. 2013, Art. no. 233001.

[19] L. Matekovits and T. S. Bird, "Width-modulated microstrip-line based mantle cloaks for thin Single- and multiple cylinders," *IEEE Trans. Antennas Propag.*, vol. 62, no. 5, pp. 2606–2615, May 2014, doi: 10.1109/TAP.2014.2307587.

[20] H. M. Bernety and A. B. Yakovlev, "Conformal and confocal mantle cloaking of elliptical cylinders using sub-wavelength metallic meshes and patches," in *Proc. IEEE Antennas Propag. Soc. Int. Symp. (APSURSI)*, Jul. 2014, pp. 1433–1434.

[21] A. Monti, J. Soric, A. Alù, F. Bilotti, A. Toscano, and L. Vegni, "Overcoming mutual blockage between neighboring dipole antennas using a low-profile patterned metasurface," *IEEE Antennas Wireless Propag. Lett.*, vol. 11, pp. 1414–1417, 2012, doi: 10.1109/LAWP.2012.2229102.

[22] J. C. Soric, A. Monti, A. Toscano, F. Bilotti, and A. Alù, "Dual-polarized reduction of dipole antenna blockage using mantle cloaks," *IEEE Trans. Antennas Propag.*, vol. 63, no. 11, pp. 4827–4834, Nov. 2015, doi: 10.1109/TAP.2015.2476468.

[23] H. M. Bernety and A. B. Yakovlev, "Reduction of mutual coupling between neighboring strip dipole antennas using confocal elliptical metasurface cloaks," *IEEE Trans. Antennas Propag.*, vol. 63, no. 4, pp. 1554–1563, Apr. 2015, doi: 10.1109/TAP.2015.2398121.

[24] H. M. Bernety and A. B. Yakovlev, "Decoupling antennas in printed technology using elliptical metasurface cloaks," *J. Appl. Phys.*, vol. 119, no. 1, Jan. 2016, Art. no. 014904, doi: 10.1063/1.4939610.

[25] S. Pawar, S. Mastromatteo, A. B. Yakovlev, H. M. Bernety, H. G. Skinner, S.-Y. Suh, and A. Alu, "Elliptical metasurface cloaks for decoupling and cloaking of microstrip monopole antennas at 28 GHz and 39 GHz for 5G wireless applications," in *Proc. IEEE Int. Symp. Antennas Propag. North Amer. Radio Sci. Meeting*, Montreal, QC, Canada, Jul. 2020, pp. 805–806.

[26] Z. H. Jiang and D. H. Werner, "Dispersion engineering of metasurfaces for dual-frequency quasi-three-dimensional cloaking of microwave radiators," *Opt. Exp.*, vol. 24, no. 9, pp. 9629–9644, May 2016, doi: 10.1364/OE.24.009629.

[27] A. Monti, J. Soric, M. Barbuto, D. Ramaccia, S. Vellucci, F. Trotta, A. Alù, A. Toscano, and F. Bilotti, "Mantle cloaking for co-site radio-frequency antennas," *Appl. Phys. Lett.*, vol. 108, no. 11, Mar. 2016, Art. no. 113502, doi: 10.1063/1.4944042.

[28] G. Moreno, A. B. Yakovlev, H. M. Bernety, D. H. Werner, H. Xin, A. Monti, F. Bilotti, and A. Alu, "Wideband elliptical metasurface cloaks in printed antenna technology," *IEEE Trans. Antennas Propag.*, vol. 66, no. 7, pp. 3512–3525, Jul. 2018, doi: 10.1109/TAP.2018.2829809.

[29] Z. Hamzavi-Zarghani, A. Yahaghi, and L. Matekovits, "Analytical design of a metasurface based mantle cloak for dielectric cylinder under oblique incidence," in *Proc. 9th Int. Symp. Telecommun. (IST)*, Tehran, Iran, Dec. 2018, pp. 65–68.

[30] H. M. Bernety, A. B. Yakovlev, H. G. Skinner, S.-Y. Suh, and A. Alu, "Decoupling and cloaking of interleaved phased antenna arrays using elliptical metasurfaces," *IEEE Trans. Antennas Propag.*, vol. 68, no. 6, pp. 4997–5002, Jun. 2020, doi: 10.1109/TAP.2019.2957286.

[31] S. Pawar, S. Mastromatteo, A. B. Yakovlev, H. M. Bernety, H. G. Skinner, S.-Y. Suh, and A. Alu, "Cloaking and decoupling of interleaved microstrip monopole arrays at 28 GHz and 39 GHz using elliptical metasurfaces for 5G wireless applications," in *Proc. IEEE Int. Symp. Antennas Propag. North Amer. Radio Sci. Meeting*, Montreal, QC, Canada, Jul. 2020, pp. 869–870.

[32] S. Pawar, H. M. Bernety, H. G. Skinner, S.-Y. Suh, A. Alù, and A. B. Yakovlev, "Mantle cloaking for decoupling of interleaved phased antenna arrays in 5G applications," in *Proc. AIP Conf.*, vol. 2300, no. 1, Dec. 2020, Art. no. 020095, doi: 10.1063/5.0031836.

[33] D. Lee and A. B. Yakovlev, "Metasurface cloaks to decouple closely spaced printed dipole antenna arrays fed by a microstrip-to-balanced transmission-line transition," *IEEE Access*, vol. 9, pp. 128209–128219, 2021, doi: 10.1109/ACCESS.2021.3112771.
[34] S. Pawar, H. G. Skinner, S.-Y. Suh, and A. B. Yakovlev, "Cloaking of slot antennas at C-band frequencies using elliptical metasurface cloaks," *IEEE Antennas Wireless Propag. Lett.*, vol. 21, no. 11, pp. 1–5, Jul. 2022, doi: 10.1109/LAWP.2022.3193038.
[35] I. F. Akyildiz and J. M. Jornet, "The Internet of Nano-Things," *IEEE Wireless Commun.*, vol. 17, no. 6, pp. 58–63, Dec. 2010.
[36] Q. Bao, H. Zhang, B. Wang, Z. Ni, C. Haley, Y. Lim, Y. Wang, D. Tang, and K. Loh, "Broadband graphene polarizer," *Nature Photon.*, vol. 5, pp. 411–415, May 2011.
[37] M. Liu, X. Yin, E. Ulin-Avila, B. Geng, T. Zentgraf, L. Ju, F. Wang, and X. Zhang, "A graphene-based broadband optical modulator," *Nature*, vol. 474, pp. 64–67, May 2011.
[38] P. Y. Chen, C. Argyropoulos, and A. Alù, "Terahertz antenna phase shifters using integrally-gated graphene transmission-lines," *IEEE Trans. Antennas Propag.*, vol. 61, no. 4, pp. 1528–1537, Apr. 2012.
[39] E. Carrasco and J. Perruisseau-Carrier, "Reflectarray antenna at terahertz using graphene," *IEEE Antennas Wireless Propag. Lett.*, vol. 12, pp. 253–256, 2013.
[40] G. W. Hanson, "Dyadic Green's functions and guided surface waves for a surface conductivity model of graphene," *J. Appl. Phys.*, vol. 103, no. 6, Mar. 2008, Art. no. 064302.
[41] P.-Y. Chen and A. Alù, "Atomically thin surface cloak using graphene monolayers," *ACS Nano*, vol. 5, no. 7, pp. 5855–5863, Jun. 2011, doi: 10.1021/nn201622e.
[42] P.-Y. Chen, J. Soric, Y. R. Padooru, H. M. Bernety, A. B. Yakovlev, and A. Alù, "Nanostructured graphene metasurface for tunable terahertz cloaking," *New J. Phys.*, vol. 15, Dec. 2013, Art. no. 123029.
[43] Y. R. Padooru, A. B. Yakovlev, C. S. R. Kaipa, G. W. Hanson, F. Medina, and F. Mesa, "Dual capacitive-inductive nature of periodic graphene patches: Transmission characteristics at low-terahertz frequencies," *Phys. Rev. B, Condens. Matter*, vol. 87, no. 11, Mar. 2013, Art. no. 115401, doi: 10.1103/physrevb.87.115401.
[44] H. M. Bernety and A. B. Yakovlev, "Cloaking of single and multiple elliptical cylinders and strips with confocal elliptical nanostructured graphene metasurface," *J. Phys., Condens. Matter*, vol. 27, no. 18, May 2015, Art. no. 185304.
[45] G. Moreno, H. M. Bernety, and A. B. Yakovlev, "Reduction of mutual coupling between strip dipole antennas at terahertz frequencies with an elliptically shaped graphene monolayer," *IEEE Antennas Wireless Propag. Lett.*, vol. 15, pp. 1533–1536, 2015, doi: 10.1109/LAWP.2015.2505333.
[46] J. Ghosh and D. Mitra, "Mutual coupling reduction in planar antenna by graphene metasurface for THz application," *J. Electromagn. Appl.* , vol. 31, no. 18, pp. 2036–2045, Dec. 2017, doi: 10.1080/09205071.2016.1277959.
[47] E. Shokati and N. Granpayeh, "Wideband cloaking by using inhomogeneous nanostructured graphene metasurface for tunable cloaking in the terahertz regime," in *Proc. 4th Int. Conf. Millimeter-Wave Terahertz Technol. (MMWaTT)*, Dec. 2016, pp. 9–13.
[48] X. Wang and S. A. Tretyakov, "Toward ultimate control of terahertz wave absorption in graphene," *IEEE Trans. Antennas Propag.*, vol. 67, no. 4, pp. 2452–2461, Apr. 2019.
[49] (2019). *CST Microwave Studio*. [Online]. Available: https://www.cst.com
[50] O. Luukkonen, C. Simovski, G. Granet, G. Goussetis, D. Lioubtchenko, A. Raisanen, and S. Tretyakov, "Simple and accurate analytical model of planar grids and high-impedance surfaces comprising metal strips or patches," *IEEE Trans. Antennas Propag.*, vol. 56, no. 6, pp. 1624–1632, Jun. 2008.
[51] C. F. Bohren and D. R. Huffman, *Absorption and Scattering of Light by Small Particles*. New York, NY, USA: Wiley. 1998.
[52] C. H. Papas, *Theory of Electromagnetic Wave Propagation*. New York, NY, USA: Dover, 1988.
[53] M. G. Silveirinha, A. Alù, and N. Engheta, "Parallel-plate metamaterials for cloaking structures," *Phys. Rev. E, Stat. Phys. Plasmas Fluids Relat. Interdiscip. Top.*, vol. 75, no. 3, Mar. 2007, Art. no. 036603, doi: 10.1103/physreve.75.036603.
[54] A. Alù, D. Rainwater, and A. Kerkhoff, "Plasmonic cloaking of cylinders: Finite length, oblique illumination and cross-polarization coupling," *New J. Phys.*, vol. 12, no. 10, Oct. 2010, Art. no. 103028, doi: 10.1088/1367-2630/12/10/103028.
[55] V. P. Chumachenko, "Domain-product technique solution for the problem of electromagnetic scattering from multiangular composite cylinders," *IEEE Trans. Antennas Propag.*, vol. 51, pp. 2845–2851, 2003.

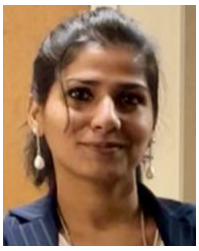

SHEFALI PAWAR (Student Member, IEEE) was born in Kolkata, India, in 1992. She received the B.E. and M.E. degrees in electronics and telecommunication engineering from the University of Mumbai, Mumbai, India, in 2015 and 2018, respectively. She is currently pursuing the Ph.D. degree in electrical engineering with The University of Mississippi, Oxford, MS, USA.

Since 2019, she has been a Research Assistant with the Department of Electrical and Computer Engineering, The University of Mississippi. Her research interests include antennas and propagation, RF and microwaves, multiband and broadband microstrip antennas, and metamaterial structures for cloaking of antennas and antenna arrays.

Ms. Pawar was a recipient of the Best Paper in Session Award at the International Conference on Computing, Communication, Control and Automation (ICCUBEA), in 2017.

HOSSEIN MEHRPOUR BERNETY (Member, IEEE) was born in Sary, Iran, in 1987. He received the B.Sc. degree in electrical engineering-communications from the Ferdowsi University of Mashhad, Mashhad, Iran, in 2010, the M.Sc. degree in electrical engineering-communications from the Babol Noshirvani University of Technology, Babol, Iran, in 2013, the M.Sc. degree in electrical engineering-electromagnetics from The University of Mississippi, Oxford, MS, USA, in 2015, and the Ph.D. degree in electrical engineering from The University of Utah, in 2020.

He is currently a Postdoctoral Scholar at Stanford University, Stanford, CA, USA. His research interests include electromagnetic scattering, cloaking, antennas, and antenna arrays.

Dr. Bernety was a recipient of the Honorable Mention Award and the Finalist Student Awards from the IEEE International Symposium on Antennas and Propagation (APS), in 2014, 2017, and 2019, respectively, and the Graduate Achievement Award from The University of Mississippi, in 2015.

ALEXANDER B. YAKOVLEV (Senior Member, IEEE) received the Ph.D. degree in radiophysics from the Institute of Radiophysics and Electronics, National Academy of Sciences, Kharkov, Ukraine, in 1992, and the Ph.D. degree in electrical engineering from the University of Wisconsin–Milwaukee, in 1997.

In summer of 2000, he joined the Department of Electrical Engineering, The University of Mississippi, as an Assistant Professor, and became an Associate Professor, in 2004. Since July 2013, he has been a Full Professor of electrical engineering. He is the coauthor of the book *Operator Theory for Electromagnetics: An Introduction* (Springer, New York, NY, USA, 2002). His research interests include mathematical methods in applied electromagnetics, homogenization theory, high-impedance surfaces for antenna applications, electromagnetic band-gap structures, metamaterial structures, wire media, graphene, cloaking, theory of leaky waves, transient fields in layered media, catastrophe, and bifurcation theories.

Dr. Yakovlev is a member of URSI Commission B. He received the Young Scientist Award at the 1992 URSI International Symposium on Electromagnetic Theory, Sydney, NSW, Australia; and the Young Scientist Award at the 1996 International Symposium on Antennas and Propagation, Chiba, Japan. In 2003, he received a Junior Faculty Research Award and a Faculty Teaching Award in the School of Engineering, The University of Mississippi, in 2017. From 2003 to 2006, he was an Associate Editor-in-Chief of the *ACES Journal*. From 2005 to 2008, he was an Associate Editor of the IEEE TRANSACTIONS ON MICROWAVE THEORY AND TECHNIQUES. Since August 2017, he has been an Associate Editor of the IEEE ANTENNAS AND WIRELESS PROPAGATION LETTERS. Since November 2019, he has been an Associate Editor of the IEEE TRANSACTIONS ON ANTENNAS AND PROPAGATION.